Soft-x-ray Kossel structures from W/C multilayers under various electron ionization conditions

P. Jonnard, J.-M. André, and C. Bonnelle

Laboratoire de Chimie Physique—Matière et Rayonnement, UMR-CNRS 7614, Université Pierre et Marie Curie,
11 Rue Pierre et Marie Curie, F-75231 Paris Cedex 05, France

F. Bridou and B. Pardo

Laboratoire Charles Fabry de l'Institut d'Optique, UMR-CNRS 8501, Bâtiment 503, Centre Scientifique d'Orsay, BP 147,
F-91403 Orsay Cedex, France

The intensity of the W $M\alpha$ line emitted by tungsten present in W/C multilayer interferential mirrors (MIM) under electron excitation is studied as a function of the detection angle of the photons. The measurements are performed for various incident-electron energies and several numbers of bilayers constituting the MIM. A spatial modulation of the x-ray intensity is observed in a domain of detection angle around the Bragg angle of the W/C multilayer for the W $M\alpha$ emission. The experimental results are compared to a model based on the reciprocity theorem using nonuniform ionization distributions. We suggest that the intensity modulation is due to the interferences between the forward and backward traveling waves inside the MIM.

I. INTRODUCTION

When a crystal is irradiated by a beam of sufficiently energetic particles, such as x-ray photons or charged particles, atomic inner-shell ionization is achieved and radiative recombination of the atoms within the crystal gives rise to characteristic x-ray emissions of wavelength λ. If the emission takes place in the Bragg direction for a set of atomic planes (hkl) of the crystal, it will be reflected at the lattice planes. The reflected radiation is spatially distributed on the surface of a cone of semiangle $\pi/2-\theta$, where θ is the Bragg angle, and on the axis normal to the hkl planes. This spatial distribution of the x-ray emission is known as Kossel structures [1,2].

The enhancement of x-ray radiation produced within a crystal, in Bragg emission directions, has attracted the interest of researchers involved in the development of x-ray sources. The basic idea is to use the phase-matched regime which takes place in the Bragg diffraction to realize a distributed-feedback laser [3], similar to the ones proposed developed in the long-wavelength domains (visible or IR domain). Indeed, the periodic structure of the crystal provides feedback by Bragg coupling between the forward- and backward-traveling waves and the crystal behaves as a spatially distributed resonator.

Yariv [4] has developed a simple model to calculate the threshold gain of an x-ray distributed-feedback laser (XDFL) in a single crystal. Coherent emission of characteristic lines on the passage of charged particles through a single crystal in connection with the quasi-Cherenkov emission was considered by Akhmanov and Grishanin [5]. Das Gupta [6,7] has observed the $K\alpha_{1,2}$ lines induced in copper crystals by electrons and detected a nonlinear rise of the intensity and a narrowing of the $K\alpha_1$ width, suggesting these changes should be due to coherent Kossel emission. The realization of a XDFL from a crystal seems difficult because it is necessary to have a natural crystal with a d-period fulfilling the Bragg condition for a wavelength emitted by the crystal.

Consequently, possibility of obtaining Bragg x-ray laser action in artificial periodic stratified media has been considered by Yariv and Yeh [8], which have shown that the quasitransparency of the medium in the vicinity of the Bragg conditions, similar to Borrman effect in crystals, should reduce significantly the pumping threshold requirement.

The advent of synthetic multilayer interferential mirrors (MIM) for which the d spacing and the nature of the materials can be arbitrarily chosen [9] has opened an opportunity in the soft x-ray domain, i.e., for radiation with wavelength larger than 1 nm. Initially the Kossel structures from MIM have been investigated under grazing conditions in the x-ray domain by means of an x-ray excitation (x-ray fluorescence): the Fe $K\alpha$ emission from a Fe/C multilayer [10] and the Ni $K\alpha$ from a Ni/C multilayer [11] have been observed. The technique has been found to be sensitive to the interface quality, thus providing a method to investigate the MIM performances. Theoretical models based on the reciprocity theorem [10] or on a matrix treatment of the wave scalar propagation in a periodic structure [11] have been used to account for the experimental results.

Recently, we have reported the first observations of oscillations in the spatial distribution of the x-ray intensity [12,13], when a characteristic emission is produced by electron excitation in MIM and the detection is made in a Bragg direction for the MIM. Experimental results have been accounted for by a simple model using the reciprocity theorem and assuming the excitation uniform in depth.

Contributions of the various parameters involved in these experiments have to be investigated. We present here a study of the spatial distribution of the W $M\alpha$ line emitted from W/C MIM as a function of the number of MIM periods and of the energy of the exciting electron beam, i.e., of the thickness in which the inner-shell ionizations take place. A model taking into account the in-depth distribution of the excitation probability by the electrons has been developed. Our main objective is to study, both experimentally and theoretically, the role of the in-depth ionization distribution and of the number of bilayers on the shape of the oscillations.

TABLE I. For the various MIM, comparison of the experimental, Δ_{expt}, and theoretical, Δ_{theor}, widths of the reflectivity curves obtained at the Cu $K\alpha$ and Cu $L\alpha$ wavelengths.

Number of	Cu $K\alpha$		Cu $L\alpha$	
bilayers	Δ_{expt} (deg)	Δ_{theor} (deg)	Δ_{expt} (deg)	Δ_{theor} (deg)
10	0.12	0.13	1.00	0.98
30	0.04	0.05	0.41	0.40
120	0.033	0.029	0.26	0.28

II. EXPERIMENT

The various W/C MIM were prepared by using a triode dc sputtering technique under a 200 Pa argon pressure. They were designed to obtain a 3 nm period, with the thickness of the W and C layers equal to 1 and 2 nm, respectively. They were deposited on silicon substrates. Several MIM having 10, 30, and 120 bilayers were prepared. These samples are called WC10, WC30, and WC120, respectively.

Measurements by x-ray reflectometry at the Cu $K\alpha$ and at the Cu $L\alpha$ wavelengths indicate a period close to 3.3 nm. The comparison of the widths of the experimental reflection curves with the theoretical ones calculated for perfect MIM is shown in the Table I. Experimental and theoretical values are in agreement, but it is not possible to obtain a good fit of the experimental reflectivity curves by using the refraction indices of pure tungsten and carbon. In fact, the theoretical reflectivity is obtained by using for each layer a weighted sum of the W and C indices. This corresponds to 55% W and 45% C (at %) for the heavy layers, and 95% C and 5% W for the light layers. Moreover, a 0.3 nm roughness is added at each interface. In addition, for the Cu $K\alpha$ wavelength, a ± 0.2 nm random variation of the thickness of the layers is introduced, but limited so that the period variation is restricted to ± 0.1 nm. In these conditions, experimental and theoretical curves are close. As an example, we present in Fig. 1 for WC30, the reflectivity measurements performed at the Cu $K\alpha$ and Cu $L\alpha$ wavelengths, compared to the theoretical reflectivities. For the Cu $L\alpha$ wavelength, the secondary structures at both sides of the main peak are not reproduced by the calculation.

We study the angular distribution of the intensity of the W $M\alpha$ emission ($4f \rightarrow 3d_{5/2}$ transition at about 1775 eV). The W $3d_{5/2}$ core shell of the tungsten atoms present in the samples are ionized by an electron beam produced from a Pierce gun (0–10 keV, 0–10 mA). The irradiated surface is about 1 cm^2, leading to a current density of a few tenths of mA/cm^2. The measurements are performed for 2.5, 4.0, and 6.0 keV incident-electron energies.

The W/C multilayers are fixed with a silver glue on the rotary sample holder. The experimental setup is such that the directions of the incident electrons and the detected photons are perpendicular. The rotation axis of the sample holder is perpendicular to the plane defined by the electron and photon directions, Fig. 2(a). This device enables the variation of the α angle between the sample surface and the direction of the detected photons. The α exit angle is varied around the Bragg angle of the W/C MIM for the W $M\alpha$ emission (about
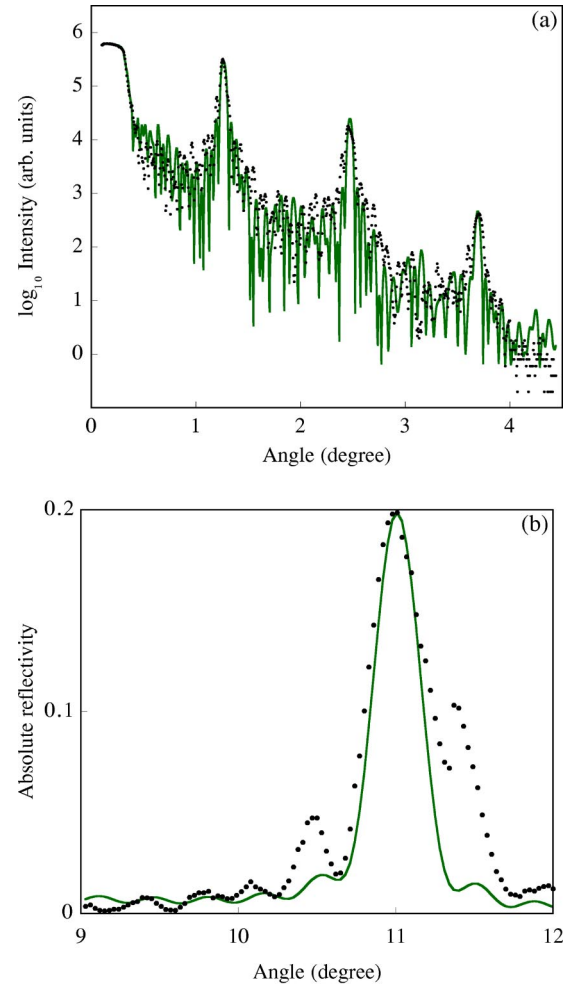
FIG. 1. (Color online) Comparison of the experimental (dots) and theoretical (line) reflectivities, obtained on the WC30 MIM, at the Cu $K\alpha$ wavelength (a) and at the Cu $L\alpha$ wavelength (b).

6.1°) with an uncertainty of $\pm 0.1°$ and the intensity is measured as a function of α.

The W $M\alpha$ emission is analyzed with a high-resolution Johann-type x-ray spectrometer [14], using an InSb (111) crystal ($d = 0.374$ nm) at the first reflection order. The spectrometer is positioned at the peak of the W $M\alpha$ emission. Because of the finite height of the irradiation area on the
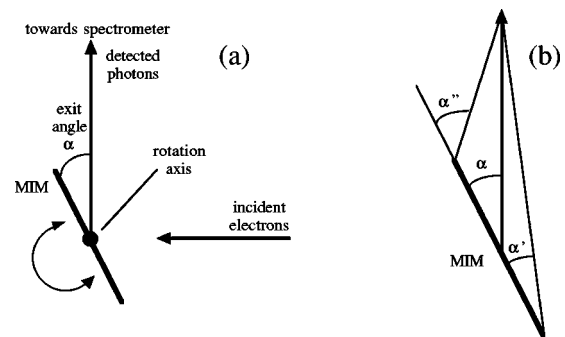
FIG. 2. (a) Geometry of the experimental setup. (b) Effect of the finite height of the sample on the detection angle: $\alpha'' > \alpha > \alpha'$.

TABLE II. For the various incident-electron energies, number of bilayers in which 90% of the W $3d_{5/2}$ ionizations are produced.

Electron energy (keV)	WC10	WC30	WC120
2.5	6	6	6
4.0	10	15	18
6.0	10	25	37

MIM (about 1 cm) and the acceptance angle of the spectrometer, there is about 0.2° between the detection angles α' and α'' measured at the ends of the MIM, when $\alpha = 6.1°$, Fig. 2(b). This spread of the α angle leads to a instrumental broadening of the angular distributions. A misorientation of the sample during the rotation could lead to an extra instrumental broadening, whose determination is cumbersome and not yet evaluated.

III. CALCULATIONS

Due to the slowing down of the electrons in solids, the in-depth distribution of the ionizations, $I(z)$, is not homogeneous inside the MIM. A semiempirical model [15] IntriX is used to estimate the depth profile of the W $3d_{5/2}$ ionizations inside the W/C MIM. The model takes into account the energy and angular distributions of the transmitted and backscattered electrons, and their ionization cross sections. For the calculations, the multilayer structure is simulated by a W_xC_y homogeneous compound having numbers of W and C atoms equivalent to that of the considered MIM.

The number of bilayers in which 90% of the ionizations are produced is indicated in Table II. For WC10 at 4 and 6 keV, the ionizations are almost uniformly distributed inside the sample. When the thickness of the sample increases, the ionization distribution is not uniform in depth. As an example, the ionization distributions inside the equivalent MIM
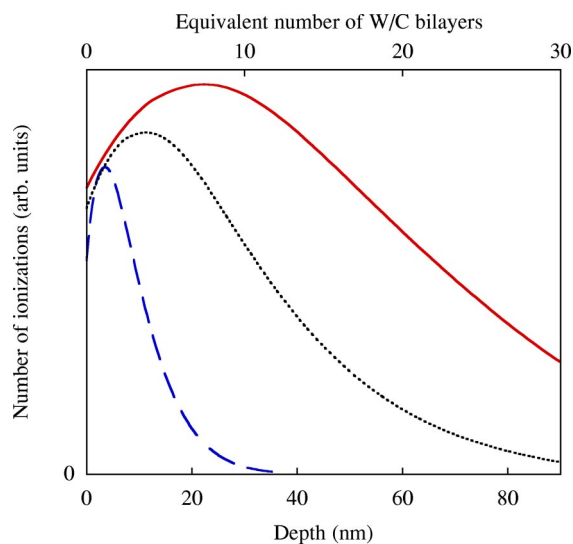
FIG. 3. (Color online) Depth distributions of the W $3d_{5/2}$ ionizations inside a WC compound having the same number of atoms than the MIM WC30: 2.5 keV (dashed line); 4.0 keV (dotted line), and 6.0 keV (solid line) electron energies.
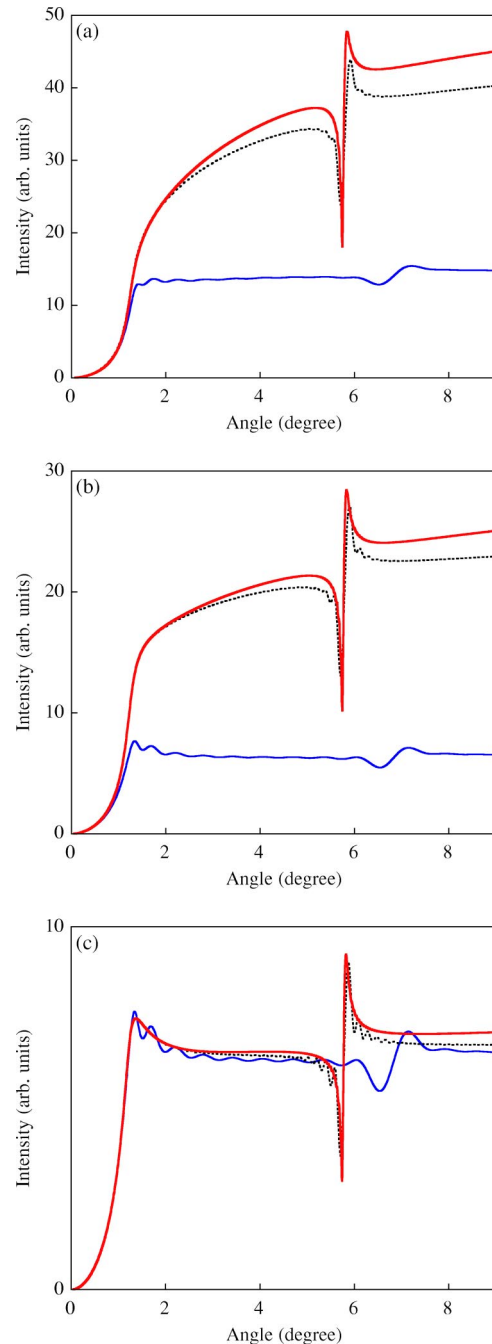
FIG. 4. (Color online) Simulated W $M\alpha$ intensity as a function of the detection angle obtained at 6.0 keV (a), 4.0 keV (b) and 2.5 keV (c). Thin solid line: WC10; dotted line: WC30; thick solid line: WC120. The W/C MIM are perfect.

WC30 is shown in Fig. 3. It can be seen that at 4 and 6 keV the electrons produce the ionizations within the whole MIM, but that the major part comes from the 15 and 25 first bilayers, respectively. The ionization distributions have been calculated for each MIM and each incident energy.

The angular distribution of the W $M\alpha$ emission is calculated with the help of a model similar to that used to describe the Bragg diffraction of the fluorescence emission in a multilayer [10]. The incident electromagnetic field is re-
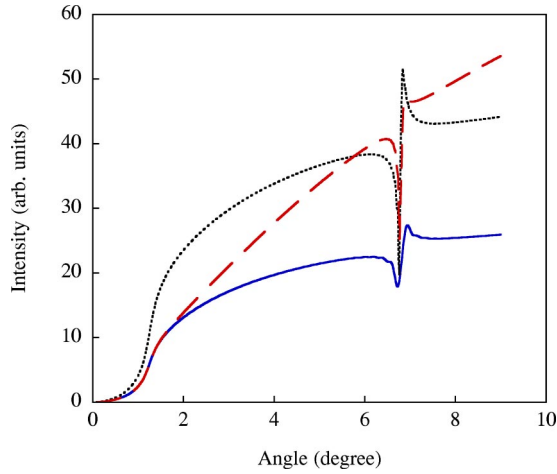
FIG. 5. (Color online) Simulations of the angular distributions of the W $M\alpha$ emission for the MIM WC120 at 6 keV electron energy, as a function of the distribution of the W $3d_{5/2}$ ionizations inside the sample. Dashed line: uniform distribution in the whole 120 bilayers; solid line: uniform distribution in the first 34 bilayers; dotted line: nonuniform distribution obtained from the IntriX semiempirical model.

placed by the square root of the in-depth distribution of the electron ionizations, $I(z)$.

The electrical field E_e, created at each point of the multilayer and arising on the detector, is calculated by using the reciprocity theorem, i.e., by considering a fictive source situated at infinity in the direction of the detector and emitting the characteristic wavelength λ. This field depends on the depth and the emergence angle θ_e. The emission intensity in the direction θ_e is proportional to

$$I(z)|E_e(\theta_e,z)|^2.$$

The intensity distribution of the W $M\alpha$ emission maximum, as a function of the exit angle $\alpha=\theta_e$, is plotted in Fig. 4 for the three incident-electron energies and three perfect MIMs, i.e., without mixing, roughness, or random variation of the thickness. With the α angle increasing, the curves present an intensity dip, followed by a large jump, then a decrease down to the background. The role of $I(z)$ on these angular distributions have been determined. As an example, the angular distributions observed from the perfect WC120 MIM at 6 keV have been calculated for three different ionization distributions: that given by the IntriX model, a constant one in all the MIM and a distribution constant only in the 34 first bilayers, then null in the rest of the MIM. The corresponding distributions are plotted Fig. 5. Noticeable changes are seen between the three curves and will be discussed hereafter.

IV. RESULTS

We present in Fig. 6 the intensity variation of the W $M\alpha$ emission as a function of the α exit angle for WC10, WC30, and WC120 samples. The curves have been adjusted with respect to the angle corresponding to the inflexion point of the intensity jump. Indeed, the Bragg angles of the various
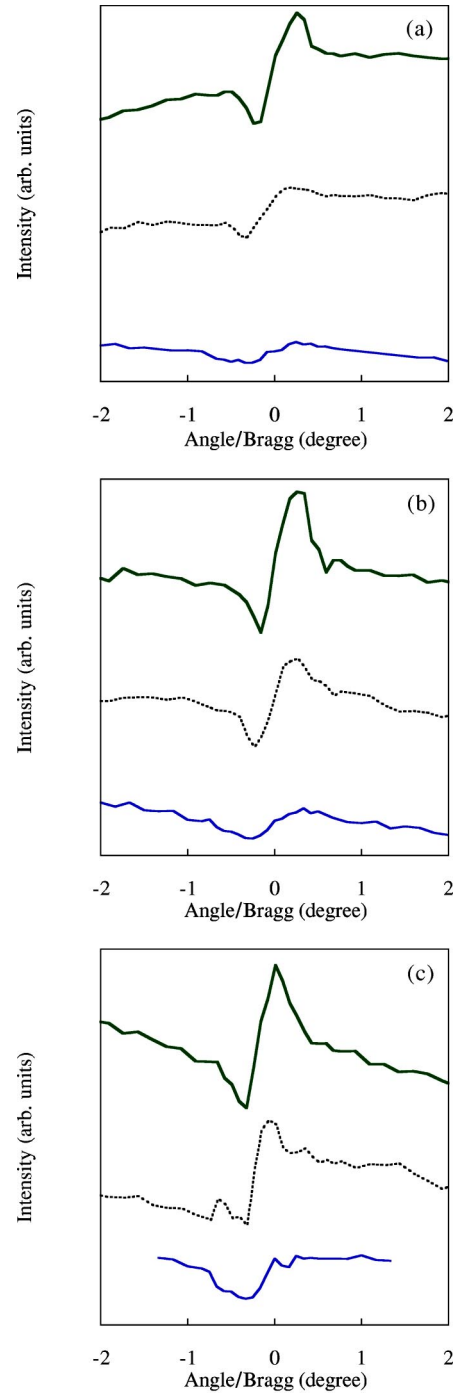
FIG. 6. (Color online) Experimental W $M\alpha$ intensity as a function of the detection angle obtained at 6.0 keV (a), 4.0 keV (b), and 2.5 keV (c). Thin solid line: WC10; dotted line: WC30; thick solid line: WC120. The curves are adjusted on the angular scale with respect to the inflexion point of the intensity offset.

MIM are not identical because the MIM do not have exactly the same period and the experimental setup does not give an absolute measurement of the exit angle. Each curve is plotted on an arbitrary intensity scale and has its own origin. As a consequence, the exact intensity and its variation with the electron energy or the number of bilayers are not considered here.

A clear modulation of the intensity is observed in all the

TABLE III. Relative amplitude, or contrast (in %), of the intensity jump of the simulated and experimental curves as a function of the detection angle, for various electron energies and for various numbers of bilayers in the MIM. The values correspond to simulated (RA_{sim}), simulated and broadened by 0.2° to take into account the experimental function, (RA_{bro}), and experimental (RA_{expt}), measurements.

Electron energy	WC10			WC30			WC120		
(keV)	RA_{sim}	RA_{bro}	RA_{expt}	RA_{sim}	RA_{bro}	RA_{expt}	RA_{sim}	RA_{bro}	RA_{expt}
2.5	17.5	17.5		47.2	26.4	22.6	89.0	35.7	25.9
4.0	12.9	12.9	7.8	40.4	25.6	17.4	71.7	27.0	21.8
6.0	12.0	12.0	8.3	34.1	23.6	16.6	72.0	26.5	20.5

experiments. Its shape is characteristic of a resonant effect: with the exit angle increasing, the intensity decreases, then increases by presenting a large intensity jump, and decreases again to get back to the background. Similar experiment performed on a thick W target shows a monotonous variation of the intensity. The inflexion point of the intensity edge is close to the Bragg angle of the W/C multilayer for the W $M\alpha$ emission. The general shape of experimental curves is in agreement with the simulated curves.

We characterize each oscillation by its ''relative amplitude,'' or contrast, defined as its peak-to-peak amplitude referred to the intensity at the inflexion point. The contrasts are estimated with an error of 0.5%. We give in Table III their values for each experiment, except for WC10 at 2.5 keV. In this case, the large slope of the background and the poor statistics do not allow a good measurement. The jump amplitude increases with the number of bilayers and decreases with increasing electron energy. The amplitude of the curve above the background, R, varies like the relative amplitude of the jump, whereas the amplitude of the curve below the background, T, is almost constant when the number of bilayers and the electron energy vary.

The contrasts deduced from the curves simulated by taking into account the atomic mixing of the MIM and by convoluting by the 0.2° experimental function, cf. Sec. II, are given in Table III. Their variation is analogous to that of the experimental contrasts but their absolute values remain

larger. This is discussed in the next paragraph. As an example, the comparison between the experimental and simulated angular distributions of the W $M\alpha$ intensity is shown in Fig. 7 for WC30 at 2.5 keV.

Another important parameter is the angular extension of the intensity modulation. To determine it, we have fitted the experimental curves by the derivatives of Gaussian or Lorentz functions plus a linear background. As an example, the fit of the curve obtained at 4 keV from WC30 is presented in Fig. 8. The best agreement is obtained for the Lorentz derivative; it is specially satisfactory in the tails before and after the intensity jump. The full widths at half maximum (FWHM) of the Lorentz curves are indicated in Table IV. They are compared to the theoretical widths, determined as the angular distance between the extrema of the curves simulated with MIM presenting mixing and convoluted by the experimental function. The theoretical values are clearly smaller than the experimental ones but their variations as a function of the incident-electron energy and the bilayer number of the MIM are analogous.

In Table V, we indicate the experimental and theoretical widths of the reflection curves at the W $M\alpha$ wavelength for the three MIM. For each number of multilayer, the experimental value is the mean of the different widths obtained with the three incident-electron energies. The simulation has been performed for perfect MIM, and for the MIM with mix-
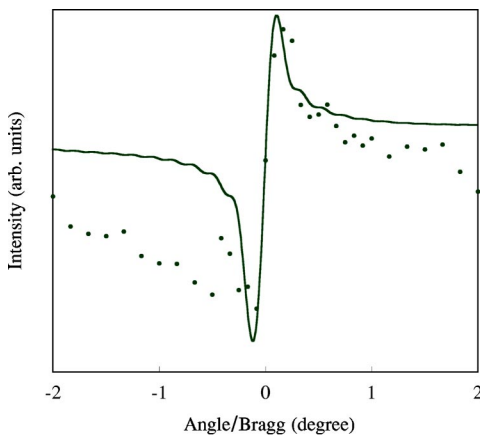
FIG. 7. Comparison of the angular distributions of the W $M\alpha$ emission for the MIM WC30 at 2.5 keV electron energy, obtained from the experiment (dots) and after the broadening by 0.2° of the simulation obtained from the MIM with mixing (line).
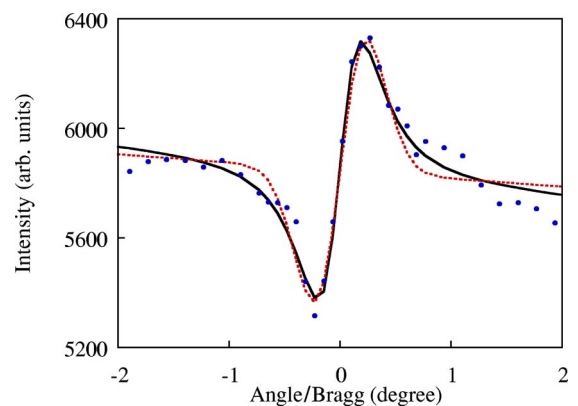
FIG. 8. (Color online) Fit of the angular distribution intensity curve obtained on WC30 and 4 keV electron energy. Dots: experiment; solid line: fit by a derivative of a Lorentz curve plus a linear background; dotted line: fit by a derivative of a Gaussian curve plus a linear background.

TABLE IV. Full width at half maximum of the Lorentz derivative function (Δ_{expt}), used to fit the angular distribution curves, for various electron energies and for various numbers of bilayers of the MIM, and full width at half maximum of the simulated, (Δ_{sim}), and simulated and broadened, (Δ_{bro}), angular distributions.

Number of bilayers	Electron energy (keV)	Δ_{expt} (deg)	Δ_{sim} (deg)	Δ_{bro} (deg)
	2.5		0.49	0.49
10	4.0	1.22	0.57	0.57
	6.0	1.34	0.58	0.58
	2.5	0.74	0.15	0.23
30	4.0	0.66	0.18	0.23
	6.0	0.88	0.19	0.25
	2.5	0.66	0.06	0.22
120	4.0	0.64	0.05	0.22
	6.0	0.62	0.06	0.21

ing. As expected, they decrease when the number of bilayers increases.

V. DISCUSSION

All the essential features of the experimental angular distributions observed for the W/C MIM are well reproduced in the calculations. The in-depth ionization distribution, used to simulate the intensity of the characteristic x-ray emission, is an important parameter in the determination of the radiation angular distribution. Various ionization distributions have been used, and we have shown that the use of the IntriX model to account for the creation of the incident radiation allows to correctly describe the shape of the angular distributions and their variation as a function of the electron energy. In contrast, a constant ionization distribution does not reproduce in a satisfactory manner the experiments (Fig. 5).

Let us consider the results obtained concerning the contrasts of the intensity jump. As can be seen from Table III, the contrasts change with the electron energy and the total number of bilayers. The most important intensity modulation is obtained for WC120 at 2.5 keV. At this energy, only the first six bilayers contribute efficiently to the W $M\alpha$ emission, whatever the total number of bilayers. The radiation

TABLE V. Experimental (Δ_{expt}) and simulated and broadened (Δ_{bro}) widths of the angular distributions obtained at the wavelength of the W $M\alpha$ emission. The Δ_{expt} values are the means of the values obtained for the three electron energies indicated in Table IV. Comparison with the theoretical widths of the reflectivity curves obtained at the W $M\alpha$ wavelength for the perfect MIMs (Δ_{theor}) and for the MIMs with mixing (Δ_{mix}).

Number of bilayers	Angular distribution		Reflectivity curve	
	Δ_{expt} (deg)	Δ_{bro} (deg)	Δ_{theor} (deg)	Δ_{mix} (deg)
10	1.28	0.55	0.50	0.46
30	0.76	0.24	0.18	0.16
120	0.64	0.22	0.08	0.05

sources are then mainly located at the top of the MIM and the forward traveling waves from these sources are reflected by the large number of bilayers situated below them. When the electron energy increases, the emission is produced deeper and deeper and the number of bilayers contributing to the reflection if the forward wave decreases. These arguments explain the changes of the relative amplitude *R*. We deduce that the amplitude of the intensity jump strongly depends on the path length of the waves in the periodic medium.

As already underlined, the variations of the experimental and theoretical contrasts are in agreement. However, the theoretical values remain larger than the experimental ones. On the other hand, the absolute values of the theoretical amplitudes decrease when the broadening effects are taken into account in the simulations. As expected, the contrasts depend on the broadening effects.

Let us now consider the experimental FWHMs determined as being the widths of the Lorentz curves whose the derivative fits the intensity oscillation. These widths weakly depend on the incident-electron energy and decrease with the number of bilayers (Table IV). They are compared in Table V to the theoretical widths, determined as the jump extension of the simulated curves, and to the widths of the reflection curves of the MIMs. All the widths vary in the same manner with the number of bilayers and a good agreement exists between the widths of the reflection curves and those deduced from the simulated curves. In contrast, the experimental FWHMs are clearly broader than the theoretical width, and the decrease of the relative amplitude can be associated with this broadening. These results suggest that supplementary experimental broadening exists. It must be underlined that the control of the broadenings is important because these effects determine the amplitude of the oscillations.

VI. CONCLUSION

Spatial oscillations of characteristic x-ray emission intensity are observed when the radiation is emitted in a periodic medium and satisfies the Bragg condition in this medium. The path length in which takes place the forward and backward traveling of the waves in the medium determines the importance of the oscillations. They also depend on the spectral resolution, i.e., on intrinsic and instrumental broadening factors, and a decrease of these factors produces an increase of the oscillation amplitude. The intensity modulation is induced in the Bragg diffraction range of the medium and the intrinsic broadening is given by the width of the Bragg reflection curve. An efficient means to enhance the importance of the intensity oscillation is to increase the resolution limit of the experiment.

Another characteristic of the Bragg reflection is the integrated intensity, i.e., the spectral intensity of the reflection range. One of the advantages of the MIM, with respect to the natural or artificial crystals, is their large integrated intensity in the soft x-ray range. That makes easier the observation of the intensity oscillations.

The primary ionization process is different depending on whether the incident particles are electrons or x-ray photons. In the case of incident photons, whose energy is constant

along the path, the ionization cross section is the same whatever the depth, whereas the electron ionization cross section varies with the electron energy, thus with the depth. If the absorption of the incident photons is weak, the radiation is emitted by the whole sample. On the other hand, the relative amplitude depends on the orientation of the incident photons with respect to the Bragg direction of the MIM for the incident wavelength. When the Bragg condition is satisfied, a regime of standing waves is set up in the MIM, and generally, each node and each antinode are located around an interface plane [16]. The characteristics of the interface have then an effect on the amplitude of the oscillation. The conditions leading to an optimal value of the amplitude, for example, conditions such that the maxima of the incident field is in the emitted layers, could be researched [8]. This effect is absent in the case of the ionization by an electron beam.

In summary, a careful study of the various parameters leading to an increase of the oscillation amplitude is necessary to expect the achievement of an x-ray resonator in MIMs.

ACKNOWLEDGMENTS

[1] W. Kossel, V. Loeck, and H. Voges, Z. Phys. **94**, 139 (1935).

[2] R.W. James, *The Optical Principles of the Diffraction of X-Rays* (Ox Bow Press, Woodbridge, CT, 1962).

[3] H. Kogelnik and C.V. Shank, Appl. Phys. Lett. **18**, 152 (1971).

[4] A. Yariv, Appl. Phys. Lett. **25**, 105 (1974).

[5] S.A. Akhmanov and B.A. Grishanin, JETP Lett. **23**, 515 (1976).

[6] K. Das Gupta, in *Physics of Quantum Electronics*, edited by S. F. Jacobs, M. Sargent III, and M.O. Scuily, Novel Sources of Coherent Radiation Vol. 5 (Addison-Wesley, Reading, MA, 1978).

[7] K. Das Gupta, Phys. Lett. A **189**, 91 (1994).

[8] A. Yariv and P. Yeh, J. Opt. Soc. Am. **67**, 438 (1977).

[9] C. Hombourger, P. Jonnard, J.-M. André, and J.-P. Chauvineau, X-Ray Spectrom. **28**, 163 (1999).

[10] J.-P. Chauvineau and F. Bridou, J. Phys. IV **6**, C7-53 (1996).

[11] H.P. Urbach and P.K. de Bokx, Phys. Rev. B **63**, 085408 (2001).

[12] P. Jonnard, J.-M. André, C. Bonnelle, and B. Pardo, in Proceedings of Physics of X-Ray Multilayer Structures, Chamonix, France, 2002 (unpublished).

[13] P. Jonnard, J.-M. André, C. Bonnelle, F. Bridou, and B. Pardo, Appl. Phys. Lett. **81**, 1524 (2002).

[14] C. Bonnelle, F. Vergand, P. Jonnard, J.-M. André, P.-F. Staub, P. Avila, P. Chargelègue, M.-F. Fontaine, D. Laporte, P. Paquier, A. Ringuenet, and B. Rodriguez, Rev. Sci. Instrum. **65**, 3466 (1994).

[15] P.-F. Staub, X-Ray Spectrom. **27**, 43 (1998); P.-F. Staub, P. Jonnard, F. Vergand, J. Thirion, and C. Bonnelle, *ibid.* **27**, 58 (1998).

[16] F. Bridou, J.-P. Chauvineau, and A. Mirone, J. Phys. IV **8**, Pr5-309 (1998).